Aerodynamic response of bridge deck under extreme climatic conditions

Sourav Ghosh[a], Rohan Das[b], Dr. Abhishek Hazra[c], Dr. Puja Halder[d],

[a]Narula Institute of Technology, Kolkata, West Bengal, India.
[b]Indian Institute of Technology Bombay, Mumbai, India.
[c]Narula Institute of Technology, Kolkata, West Bengal, India.
[d]Sanak Educational Trust's Group of Institutions Kolkata, West Bengal, India.

Abstract

The aerodynamic response of the bridge deck has received a lot of attention throughout the last few decades. Wind and surrounding climatic conditions play a vital role in shaping the aerodynamic response of infrastructures such as long-span bridges, wind turbines, skyscrapers, and other tall or slender structures. Long-span bridges are one of the most critical infrastructures influenced by wind due to their large surface areas and flexible structural systems. The harsh climatic conditions create a hostile and challenging environment for developing and maintaining long-span bridges, which are essential for efficient transportation, user safety, infrastructure reliability, convenience, and sustained economic growth in many regions. This study investigates the aerodynamic response of bridge decks under extreme climatic conditions through advanced numerical and experimental techniques. The High-Reynolds k-ε turbulence model, along with Sutherland's formula for temperature-dependent viscosity, was used in the analysis to capture complex fluid-structure interactions. This numerical method was employed to enhance the accuracy and reliability of the simulation results. A wide range of climatic parameters was considered from extreme geographical locations, including wind speed, dynamic viscosity, ambient temperature, turbulence intensity, air density, and angle of attack on the bridge deck surface. Wind tunnel simulations supported by a high-fidelity computational fluid dynamics (CFD) model were conducted throughout the study. The investigation presents a detailed analysis of airflow patterns, pressure distribution, boundary layer effects, and vortex shedding mechanisms around the bridge deck under extreme environmental loading. Throughout the analysis, it was consistently observed that wind turbulence, gustiness, and fluctuating flow fields significantly affect the dynamic response of the deck, often triggering aeroelastic instabilities such as large-scale vortex formation, flutter, and galloping. The result offers a global perspective on how various environmental and aerodynamic factors impact bridge deck performance, longevity, and safety under increasingly volatile climatic conditions.

Keywords: Climate resilient, Bridge deck, Aerodynamics, Vortex, Harsh climate

1. Introduction

In this realm of civil engineering, developing long-span bridges is one of the significant evolutions. This infrastructure enables efficient transportation across geographical barriers such as valleys, rivers, and straits. The growth of population and urbanization has intensified, and the demand for longer, sustainable, and aesthetically refined bridge structures has increased. With the demand for advancement in infrastructural revolution, there comes a lot of challenges for ensuring that the structure shall not only withstand the static load but also shall deal with the complex dynamic loading under different environmental factors, especially for the induced wind influenced by the climate [1]. A comprehensive study was done to analyse

the coupled dynamics of bridges, vehicles, and wind, providing valuable insights into the synergistic interaction of these systems under real-world conditions. The study presents an analytical framework that illustrates the dynamic interaction between the train and bridge system under the influence of wind. It highlights that, in some cases, the intensity of vibrations induced by wind forces can surpass those generated by the moving train itself. This finding underscores the critical importance of thoroughly considering wind effects when evaluating the structural response of bridges during train passage. As trains traverse bridges, especially in regions prone to strong or fluctuating winds, the combined dynamic loads from both wind and train movement can significantly affect the stability and safety of the structure. Therefore, integrating wind-induced dynamics into the overall analysis is essential for the accurate assessment and design of train-bridge systems. (C.D. Montaya et al. 2021) [2] has conducted a study on the aerodynamic performance of twin-box bridge decks has become a critical research area, particularly due to the complex interplay between deck geometry, gap distance, and aeroelastic phenomena like flutter and buffeting he additionally mentioned the previous studies of (e.g., Qin et al., 2007; Yang et al., 2015; Alvarez et al., 2018) on aerodynamic responses, which emphasizes the sensitivity of aerodynamic responses to the gap-to-depth ratio, identifying thresholds beyond which flow patterns and vortex dynamics shift significantly. Their integration into long-span bridge design remains recent. [3] (A. A. Estébanez, 2017) analyzed the coupled dynamics of vehicles, bridges, and wind. This pioneered approach integrates aerodynamic forces acting on both the bridge and the moving vehicles, reflecting real-world interactions. It significantly improves the accuracy of safety and structural performance evaluations, especially for long-span bridges subjected to strong or unsteady wind conditions. [4] Revealed that the key train-bridge wind interactions. Subsequent researchers expanded on this through wind tunnel experiments, analyzing airflow and pressure distribution around stationary vehicle-bridge systems under varying wind conditions. These studies improved understanding of wind effects and informed safer bridge design. Additionally, various countermeasures have been developed to mitigate adverse aerodynamic impacts in high-wind. [5] Apart from the aerodynamic force measurements, various countermeasures have been evolved so far to dominate the aerodynamic effect. However, studies on fluter analysis for the deck have often been overlooked, which is vital for the study. emphasised that the more economical design for a long-span bridge is using an steel twin box grider STBG without any appendages. Another mechanism is buffeting, which is affected by the gap distances. Earlier studies are evidence of the lots of research with STBG. Still, little research was conducted considering all the parameters for enhancing STBG capability by nullifying its loophole. However, in the context of pressure and frictional drag studies, very few quantities of parametric analyses were conducted.

2. Methodology

The study elaborates that the total aerodynamic (F_{DT}) acting on the bridge deck is decomposed and distinguished into different components, pressure drag force (F_{DP}) and frictional drag force (F_{DF}) acting upon the bridge deck. In this section, we can understand that the drag force (F_D), lift force (F_L), and moments (M) are easy to compute by numerical simulation. Those forces are used to analyse the drag force coefficient (C_D), lift force coefficient (C_L), and moment coefficient (C_M). Fig.4 mentions the different components of force where (F_H) is horizontal force, (F_V) is vertical force, (F_D) is drag force, (F_L) is lift force, M is moment, and α is the angle of attack. [25], The equation 1 below defines the total force (F_{DT}) applied on the deck is the

sum of pressure drag force (F_{DP}) and frictional drag force (F_{DF}), which can be further break into equation 2, 3 & 4 where the abbreviation denotes the following symbols, pressure drag coefficient concerning angle of attack ($C_{DP}(\alpha)$), frictional drag coefficient concerning angle of attack ($C_{DF}(\alpha)$), depth of the deck D, span of the bridge is L, breath of deck B, drag coefficient concerning the angle of attack $C_D(\alpha)$, tributary length (ΔLi), mean pressure (pi), shear stress parallel to the direction of drag force (six), monitoring point (i), total monitoring points (n), and the angle between the vertical axis and pressure direction (Hi). Finally, by simplifying the equations, we get the formula of $C_D(\alpha)$, $C_{DP}(\alpha)$, $C_L(\alpha)$, and $C_M(\alpha)$ mentioned in equations 5, 6, 7, and 8. The equations of forces are simplified to understand the contribution of forces across different flow conditions, direction, and geometrical configurations, creating an analytical formula of aerodynamic performance around different design scenarios.

$$F_{DT} = F_{DP} + F_{DF}$$

$$= 0.5\rho U^2 C_{DP}(\alpha) DL + 0.5\rho U^2 C_{DF}(\alpha) DL \quad (1)$$

$$F_{DT} = 0.5\rho U^2 C_D(\alpha) DL \quad (2)$$

$$F_{DP} = \sum_{i=1}^{n} P_i \Delta L_i \sin\theta_i \quad (3)$$

$$F_{DF} = \sum_{i=1}^{n} \tau_{iX} \Delta L_i \quad (4)$$

$$C_D(\alpha) = \frac{F_{DT}}{0.5\rho U^2 DL} \quad (5)$$

$$C_{DP}(\alpha) = \frac{F_{DP}}{0.5\rho U^2 DL} \quad (6)$$

$$C_L(\alpha) = \frac{F_L}{0.5\rho U^2 BL} \quad (7)$$

$$C_M(\alpha) = \frac{M}{0.5\rho U^2 BL} \quad (8)$$

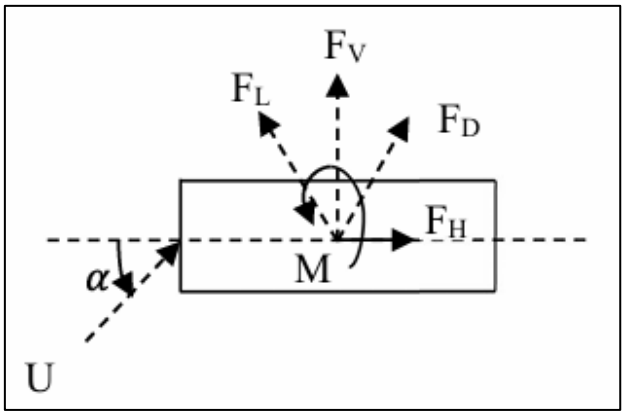

Figure 1. Aerodynamic Forces diagram (P. Haldar & S. Karmakar (2023))

2.1. Validation

The validation was done by comparing the analytical results with the results of (P. Haldar & S. Karmakar (2023)) [6] C_D, C_F, and C_M graph mentioned in fig. 2 was taken from [6]. The results of C_D, C_L, and C_M have not matched, but have come close enough at the different angle of attack. The analysis was done in ANSYS Fluent. The points where the result matches the reference given below in Fig. 3

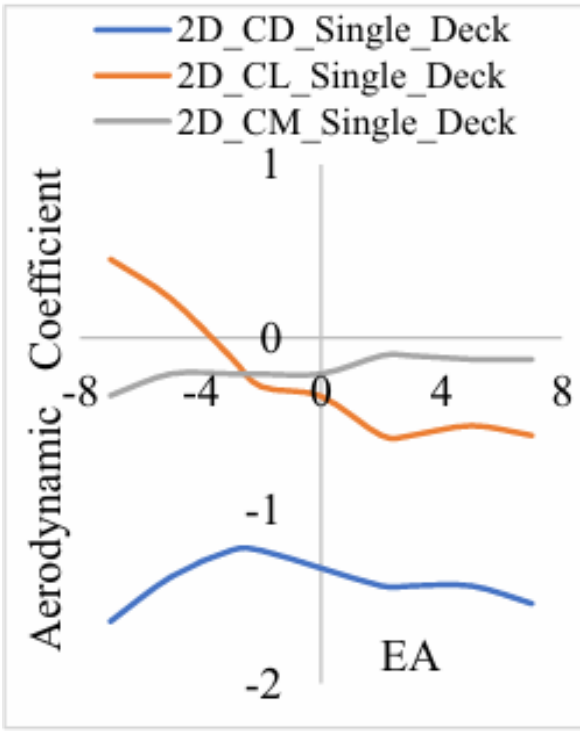

Figure 2. Aerodynamic coefficient graph image (P. Haldar & S. Karmakar (2023))

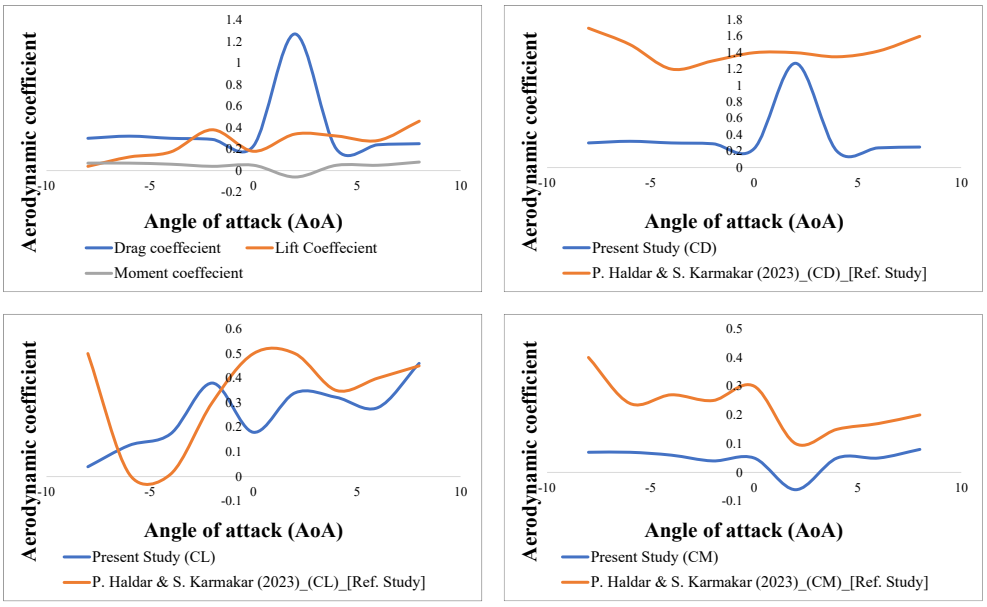

<u>Figure 3. Comparison of aerodynamic coefficients (CD, CL, CM) with angle of attack (AoA). Top-left: results from present study; others: validation against P. Haldar & S. Karmakar (2023).</u>

2.2. The governing equations used throughout the model for analysis.

The two-equation turbulence models are widely used in fluid dynamics because they solve two separate equations to estimate both the turbulent length scale and the turbulent time scale, which are key to describing turbulence behavior. The standard k-ε model in ANSYS Fluent is a popular example for analysis, originally developed by Launder and Spalding. It has become a standard tool in engineering simulations due to its robustness, cost-effectiveness, and good accuracy for a wide variety of turbulent flow and heat transfer problems. The model is semi-empirical, meaning its equations are based partly on theoretical reasoning and partly on experimental data [7].

The standard k-ε turbulence model is based on two transport equations: one for turbulent kinetic energy (k) and one for its dissipation rate (ε). The equation for k is derived directly from the exact form of the Navier–Stokes equations. However, the equation for ε is not derived mathematically, but rather developed using physical intuition and empirical adjustments, and it does not closely resemble the exact mathematical formulation [7].

In deriving the standard k-ε turbulence model, it is assumed that the flow is fully turbulent or the effects of molecular viscosity are negligible compared to turbulent effects. As a result, the model is designed to simulate fully developed turbulent flows and is not valid for laminar or transitional flow regimes where molecular viscosity plays a significant role.

As the strengths and limitations of the standard k-ε turbulence model became better understood, researchers introduced modifications to enhance its performance for a wider range of flow conditions. Two such improved variants are available in ANSYS Fluent:

RNG k-ε Model [8]: Based on Renormalization Group (RNG) theory, this model includes additional terms that improve accuracy for flows with high strain rates, swirling flows, and transitional regimes.

Realizable k-ε Model [8]: This version ensures that the model adheres to certain physical constraints (realizability conditions), improving predictions for boundary layer flows, separation, and recirculation zones

- kinetic energy (k) equation:

$$\frac{\partial(\rho k)}{\partial t} + \frac{\partial(\rho k U_i)}{\partial x_i} = \frac{\partial}{\partial x_j}\left[\left(\mu + \frac{\mu_t}{\sigma_k}\right)\frac{\partial k}{\partial x_j}\right] + G_k + G_b - \rho\varepsilon - Y_M + S_k \quad (9)$$

- Turbulent dissipation rate (ε) equation:

$$\frac{\partial(\rho \varepsilon)}{\partial t} + \frac{\partial(\rho \varepsilon U_i)}{\partial x_i} = \frac{\partial}{\partial x_j}\left[\left(\mu + \frac{\mu_t}{\sigma_\varepsilon}\right)\frac{\partial \varepsilon}{\partial x_j}\right] + G_{1\varepsilon}\frac{\varepsilon}{k}(G_k + C_{3\varepsilon}G_b) - C_{2\varepsilon}\rho\frac{\varepsilon^2}{k} + S_\varepsilon \quad (10)$$

Where:

ρ: fluid density

U_i: velocity component in the i-th direction

μ: dynamic viscosity

μ_t: turbulent (eddy) viscosity

$\sigma_k, \sigma_\varepsilon$: turbulent Prandtl numbers for k and ε

G_k: generation of turbulence kinetic energy due to mean velocity gradients

G_b: generation of turbulence kinetic energy due to buoyancy

Y_M: contribution of fluctuating dilatation in compressible turbulence to the overall dissipation rate

S_k, S_ε: user-defined sore terms

$C_{1\varepsilon}, C_{2\varepsilon}, C_{3\varepsilon}$: model constants

- The turbulent (eddy) viscosity μ_t Is modeled as:

$$\mu_t = \rho C_\mu \frac{k^2}{\varepsilon} \tag{11}$$

- The following standard model constants:

$C_\mu = 0.09$

$\sigma_k = 1$

$\sigma_\varepsilon = 1.3$

$C_{1\varepsilon} = 1.44$

$C_{2\varepsilon} = 1.92$

2.3 Dimension of the deck

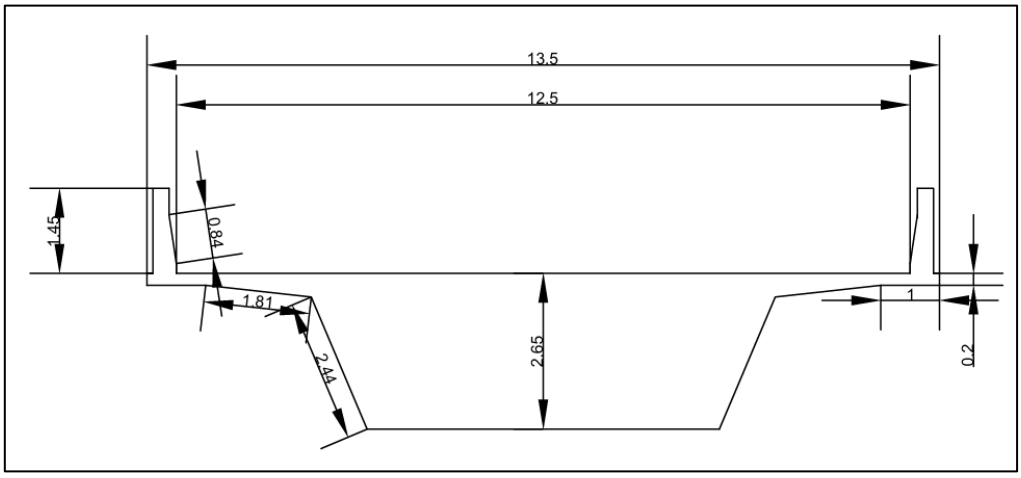

Figure 4. Dimensions of the deck (unit m)

The geometry of this bridge deck was adopted from (P. Haldar & S. Karmakar (2023)) [6]. The RC trapezoidal box girder is commonly used in long-span bridges due to its favourable

aerodynamic performance. The characteristic width of the deck is denoted as 13.5 m, which serves as the reference length scale throughout the analysis. All other geometric parameters, including the height of the deck, slope angles, and edge configurations were scaled proportionally based on the referenced study. This approach allows for a validated comparison of aerodynamic behaviour, including pressure distribution, vortex shedding, and lift and drag coefficients, under similar conditions.

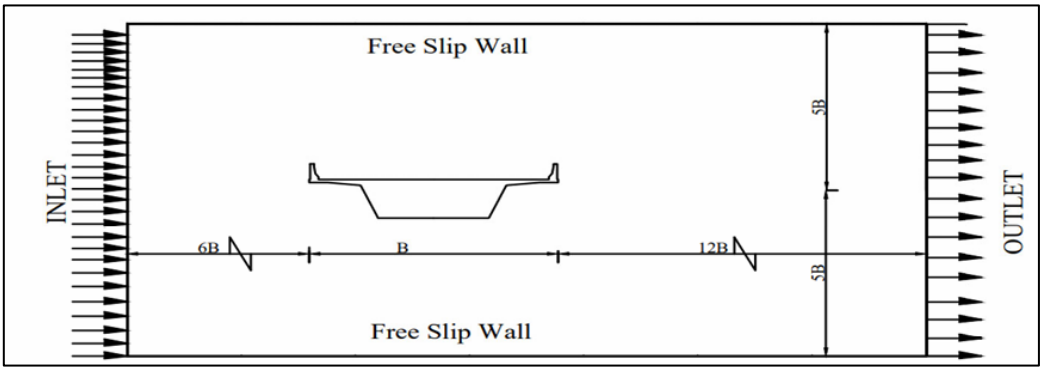

Figure 5. dimension of the flow domain (P. Haldar & S. Karmakar (2023))

The flow domain was also designed according to [6] (P. Haldar & S. Karmakar (2023)), and the mesh size was taken as 750 mm because it yielded the results that closely match the expected result needed for validation.

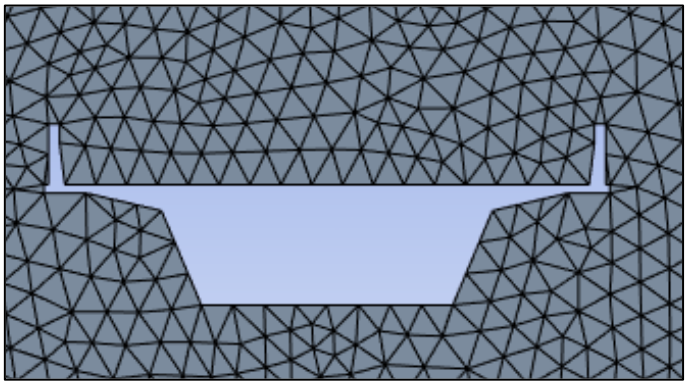

Figure 6. Different angle of attack of the deck

2.4 Air modelling

The air pressure was designed according to Sutherland's formula

A temperature-dependent model is used to calculate the dynamic viscosity of gases more accurately than using a constant value, for accuracy.

The equation is represented as:

$$\mu(T) = \mu_0 \left(\frac{T}{T_0}\right)^{\frac{3}{2}} \times \frac{T_0+S}{T+S} \quad (14)$$

$\mu(T)$ Dynamic viscosity at temperature T

μ_0 Reference viscosity at reference temperature T_0

T Local temperature (in Kelvin)

T_0 Reference temperature

S Sutherland constant (for air: ~110.4 K)

2.5 Climatic conditions

Table 1. Climatic conditions considered for the analysis and their reference

Nation	Density Kg/m^3	wind speed m/s	Dynamic viscosity Kg/Ms	Temp °C	Turbulence %	Source
Antarctica	1.225	90.8	1.81E-05	-89	80	Australian Antarctic program A&A – Atmospheric turbulence at the South Pole [9]
Arctic Circle	1.6	5.5	1.71E-05	0	50	Engineers edge Journal of Geophysical Research: Atmospheres The Engineering tool box Springer arctic boundary layer turbulence [10] & Climate.gov
Sahara Desert	1.204	3	1.81E-05	47	60	Nasa earth observatory Engineering edge Windi.app AMS Journal – Saharan boundary layer turbulence [11]

Most of the data on climatic conditions mentioned in table 1 are taken from the website

1. Australian Antarctic program - (https://www.antarctica.gov.au/about-antarctica/weather-and-climate/weather/)

2. Engineers edge - (https://www.engineersedge.com/physics/viscosity_of_air_dynamic_and_kinematic_14483.htm)

3. The engineering toolbox - (https://www.engineeringtoolbox.com/air-density-specific-weight-d_600.html)

4. Climate.gov - (https://www.climate.gov/news-features/understanding-climate/climate-change-arctic)

5. Nasa earth observary - (https://earthobservatory.nasa.gov/biome/biodesert.php)

6. Engineering edge - (https://www.engineersedge.com/physics/viscosity_of_air_dynamic_and_kinematic_14483.htm)

7. Windi.app - (https://windy.app/forecast2/spot/1975775/Sahara+Marine)

3. Results and discussions

3.1 Aerodynamic coefficient and forces

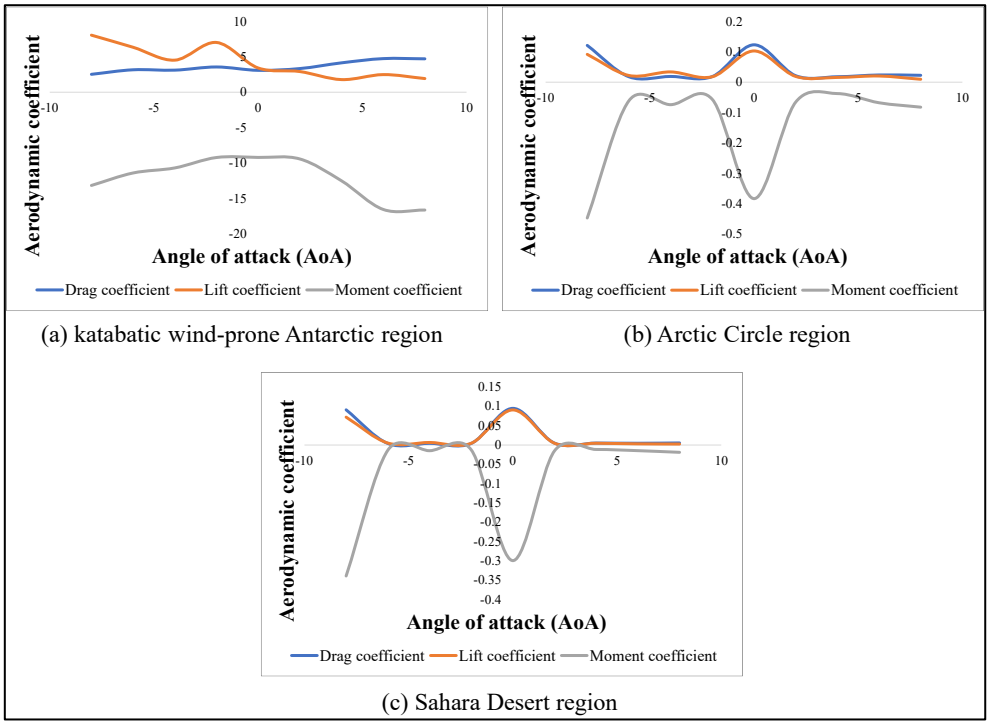

Figure 7. Variation of aerodynamic coefficients (CD, CL, CM) with angle of attack (AoA) for different regions analyzed in the present study.

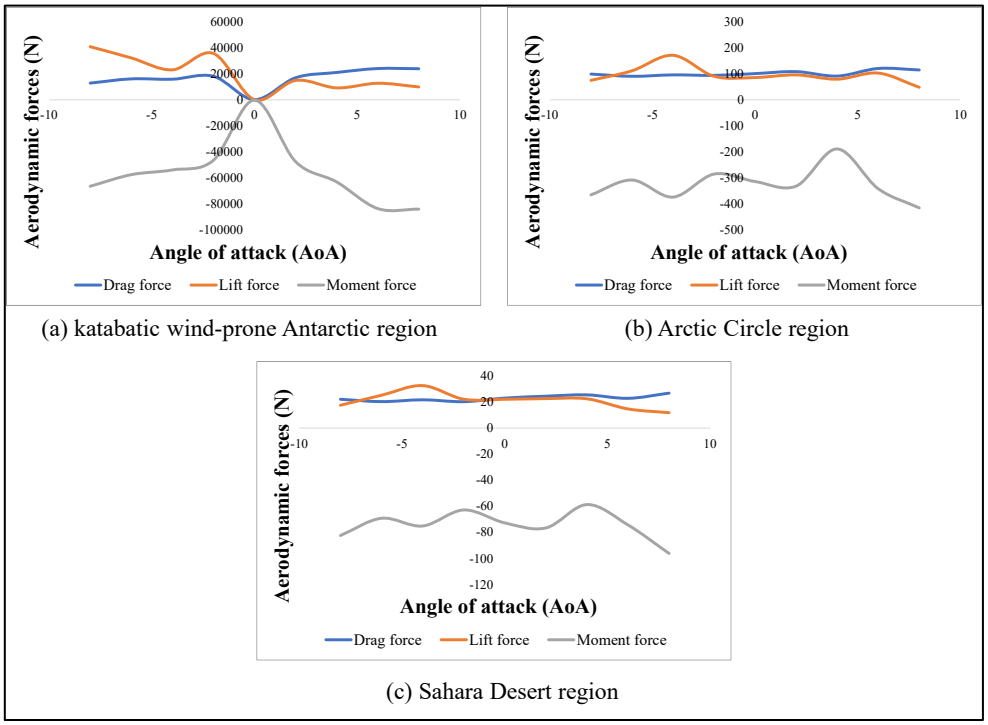

Figure 8. Variation of aerodynamic forces (CD, CL, CM) with angle of attack (AoA) for different regions analyzed in the present study.

Figure 8&7 illustrates the variation of aerodynamic forces and coefficients acting on a bridge deck. The drag, lift, and moment acting on a bridge deck under extreme climatic conditions, in various angles of attack (-8° to +8°). The fig. 8 & 7 both are divided in three distinct subplots according to the climates of Antarctica, the Arctic Circle, and the Sahara Desert.

Fig. 8a represents the express the combination of extreme wind speed (90.8 m/s), with a turbulence of 80%, temperature of -89° C, and density of 1.225kg/m^3 mentioned in table. 1. This combination leads to large aerodynamic force, especially the moment that peaked in +6° angle of attack and drag force that peaked in -8°, posing a threat to aeroelastic stability, conversely, in arctic region the forces are moderate (fig. 8b). The curve in the graph exhibits smooth transition, reflecting relatively stable aerodynamic behavior. In the fig. 8c Shara dessert shows the lowest magnitude of aerodynamic forces due to low wind speed and low air density associated with high ambient temperatures around 47° C. Here drag, lift, and moment forces showed very gentle result with respect to different the angle of attack, indicating a less critical aerodynamic environment.

Fig. 7a represents the express the combination of extreme wind speed (90.8 m/s), with a turbulence of 80%, temperature of -89° C, and density of 1.225kg/m^3 mentioned in table. 1. This combination leads to large aerodynamic coeffecients, especially the moment that peaked in +8° angle of attack and lift force that peaked in -8°, posing a threat to aeroelastic stability, conversely, in arctic region the forces are moderate (fig. 8b) except the moment at -8° of attack, that spiked unexpectedly. In the fig. 8c Shara dessert shows the lowest coefficient as usually of due to low wind speed and low air density associated with high ambient temperatures around 47° C.

3.2 Pressure contour lines indicating the vortex formation

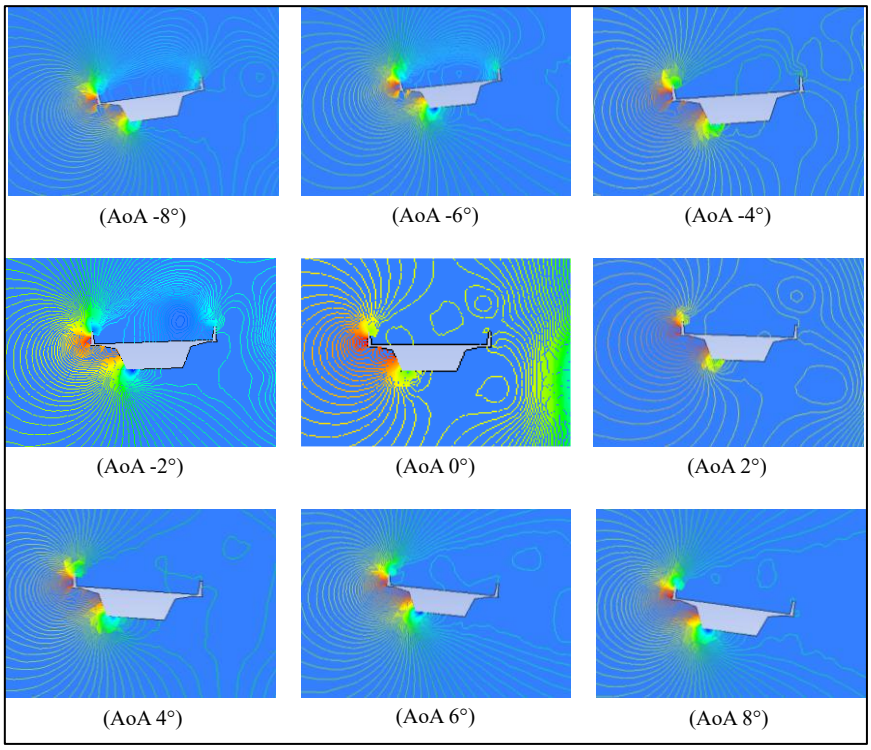

Figure 9. 2D pressure contour visualizations at various angles of attack, representing wind-induced pressure variations from ANSYS Fluent simulations (Antarctic climate).

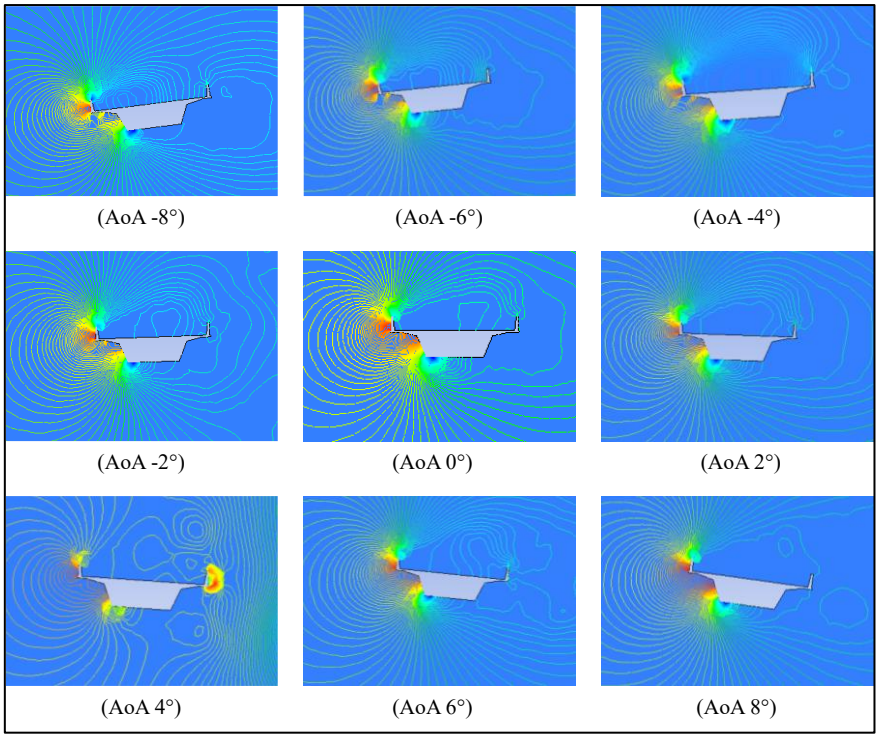

Figure 10. 2D pressure contour visualizations at various angles of attack, representing wind-induced pressure variations from ANSYS Fluent simulations (Arctic Circle climate).

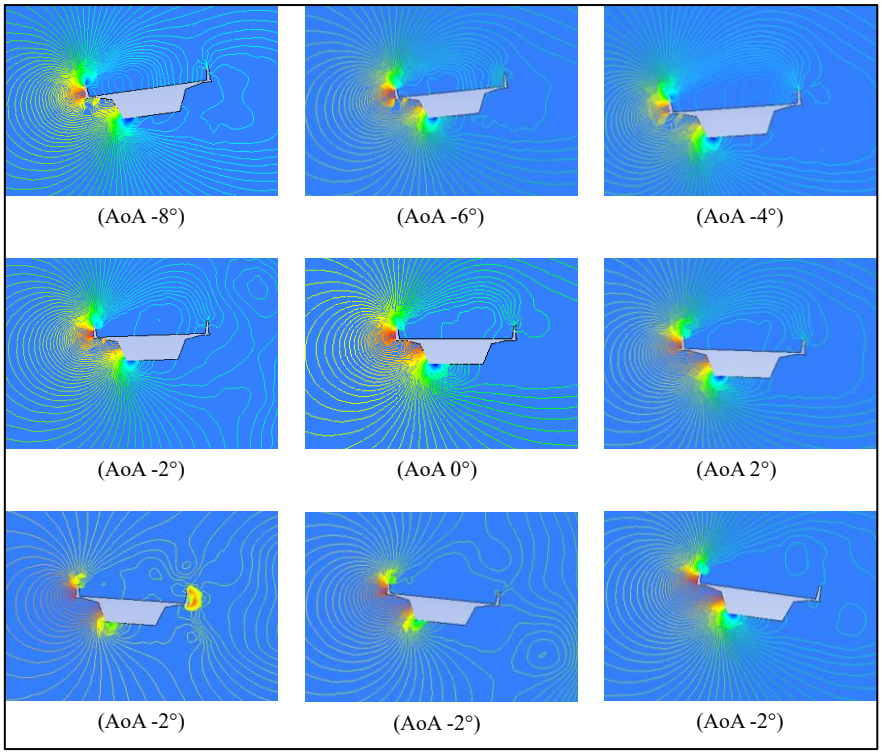

Figure 11. 2D pressure contour visualizations at various angles of attack, representing wind-induced pressure variations from ANSYS Fluent simulations (Sahara Desert climatic).

Fig. 9, 10, and 11 emphasizes 2D pressure contour plots generated from ANSYS Fluent simulations. It reveals how airflow behaves around the bridge deck at different angles of attack under distinct climatic conditions, Katabatic region of Antarctica, Arctic Circle, and Sahara Desert, respectively. In fig. 9 (Antarctica), the contours display intense pressure differentials and prominent vortex formations, particularly at higher angles of attack, which correspond to the high aerodynamic forces and coefficients seen in earlier graphs. This reflects the influence of strong katabatic winds and dense air typical of Antarctic conditions. fig. 10 (Arctic) shows moderately intense pressure variations and more streamlined flow separation, indicating a transitional aerodynamic response neither as extreme as Antarctica nor as stable as the Sahara. In fig. 11 (Sahara Desert), the pressure contours are smoother and more uniform, with weaker vortex formation and lower pressure gradients, aligning with the low aerodynamic coefficients and forces caused by hot, less dense desert air. Collectively, these visualizations reinforce the numerical findings, offering physical insight into how airflow patterns and pressure zones vary under climate-specific conditions, directly influencing bridge deck stability and performance.

3. Conclusion

This study investigates the aerodynamic performance of a reinforced concrete trapezoidal box girder bridge deck under the influence of extreme climatic conditions using validated CFD simulations. By incorporating realistic environmental parameters from three distinct geographical regions: the Katabatic region of Antarctica, Arctic Circle, and Sahara Desert. The research offers a global perspective on how temperature, wind speed, air density, viscosity, and turbulence levels interact to affect aerodynamic behaviour.

The simulation results demonstrate how climatic variations like, wind speed, air density, temperature, and turbulence intensity influence aerodynamic coefficients and force responses. The Katabatic wind-prone Antarctic region region, exhibits high wind speeds and dense cold air, exhibited the most severe aerodynamic effects, while the Sahara exhibited milder effects attributed to its hot, low-density atmosphere. The Arctic region presented intermediate behavior, illustrating its smooth transitional climatic characteristics.

Moreover, the 2D pressure contour lines indicate that the formation of vortices and pressure differentials at different angles of attack align well with the numerical trends observed in coefficient and force diagrams. This cross-validation between visualized flow behaviour and numerical outputs supports the robustness of the employed simulation methodology.

The research also implements the critical importance of incorporating localized climatic data into bridge aerodynamic design, as reliance on standard code-based assumptions may underestimate the dynamic wind-induced responses in extreme environments. The findings advocate for site-specific aerodynamic assessments and resilience-oriented design strategies, especially for infrastructure in climate-sensitive or remote regions.

In conclusion, the study not only enhances the current understanding of aerodynamic behavior under varying environmental conditions but also contributes valuable insights for future climate-resilient bridge design practices.

CRediT authorship contribution statement

Sourav Ghosh: Writing – original draft, Visualization, Validation, Software, Resources, Methodology, Investigation, Formal analysis, Data curation, Conceptualization.
Rohan Das: Writing – original draft, Writing – review & editing.
Dr. Abhishek Hazra: Writing – review & editing, Supervision.
Dr. Puja Halder: Writing – review & editing, Supervision

Declaration of competing interest

The authors declare that they have no known competing financial interests or personal relationships that could have appeared to influence the work reported in this paper.

Data availability

Data will be made available on request.

Reference

[1] Y. L. Xu and W. H. Guo, 'Dynamic analysis of coupled road vehicle and cable-stayed bridge systems under turbulent wind', *Eng Struct*, vol. 25, no. 4, pp. 473–486, 2003, doi: 10.1016/S0141-0296(02)00188-8.

[2] M. Cid Montoya, F. Nieto, S. Hernández, A. Fontán, J. A. Jurado, and A. Kareem, 'Optimization of bridges with short gap streamlined twin-box decks considering structural, flutter and buffeting performance', *Journal of Wind Engineering and Industrial Aerodynamics*, vol. 208, Jan. 2021, doi: 10.1016/j.jweia.2020.104316.

[3] A. Alonso-Estébanez, J. J. Del Coz Díaz, F. P. Álvarez Rabanal, and P. Pascual-Muñoz, 'Numerical simulation of bus aerodynamics on several classes of bridge decks', *Engineering Applications of Computational Fluid Mechanics*, vol. 11, no. 1, pp. 435–449, Jul. 2017, doi: 10.1080/19942060.2016.1201544.

[4] M. A. Barcala and J. Meseguer, 'An experimental study of the influence of parapets on the aerodynamic loads under cross wind on a two-dimensional model of a railway vehicle on a bridge', *Proc Inst Mech Eng F J Rail Rapid Transit*, vol. 221, no. 4, pp. 487–494, 2007, doi: 10.1243/09544097JRRT53.

[5] M. W. Sarwar and T. Ishihara, 'Numerical study on suppression of vortex-induced vibrations of box girder bridge section by aerodynamic countermeasures', *Journal of Wind Engineering and Industrial Aerodynamics*, vol. 98, no. 12, pp. 701–711, 2010, doi: 10.1016/j.jweia.2010.06.001.

[6] P. Haldar and S. Karmakar, 'Wind response on RC trapezoidal box girder bridge using computational fluid dynamics', doi: 10.1007/s12046-023-02127-xS.

[7] A. Weber, H.-J. Bart, and A. Klar, 'Simulating Spiraling Bubble Movement in the EL Approach', *Open Journal of Fluid Dynamics*, vol. 07, no. 03, pp. 288–309, 2017, doi: 10.4236/ojfd.2017.73019.

[8] T. Shih, W. Liou, A. Shabbir, Z. Yang, and J. Zhu, 'A New k-e Eddy Viscosity Model for High Reynolds Number Turbulent Flows-Model Development and Validation A NEW k-EPSILON EODY VISCOSITY MODEL FOR HIGH REYNOLDS NUMBER TURBULENT FLOWS: MODEL DEVELOPMENT AND VALIDATION Uncl as', 1994.

[9] T. Travouillon, M. C. B. Ashley, M. G. Burton, J. W. V. Storey, and R. F. Loewenstein, 'Atmospheric turbulence at the South Pole and its implications for astronomy', *Astron Astrophys*, vol. 400, no. 3, pp. 1163–1172, 2003, doi: 10.1051/0004-6361:20021814.

[10] B. J. Butterworth, G. de Boer, and D. Lawrence, ‘A Study of Intermittent Turbulence in Stable Arctic Boundary Layers’, *Boundary Layer Meteorol*, vol. 190, no. 1, Jan. 2024, doi: 10.1007/s10546-023-00847-5.

[11] L. Garcia-Carreras *et al.*, ‘The turbulent structure and diurnal growth of the Saharan atmospheric boundary layer’, *J Atmos Sci*, vol. 72, no. 2, pp. 693–713, 2015, doi: 10.1175/JAS-D-13-0384.1.